Supporting Online Material for

An fMRI-based biomarker for physical pain

Tor D. Wager[1]
Lauren Y. Atlas[2]
Martin A. Lindquist[3]
Mathieu Roy[1]
Choong-Wan Woo[1]
Ethan Kross[4]

[1] Department of Psychology and Neuroscience, University of Colorado, Boulder
[2] Department of Psychology, New York University
[3] Department of Statistics, Columbia University
[4] Department of Psychology, University of Michigan

Correspondence to:
Tor D. Wager
Department of Psychology and Neuroscience
University of Colorado, Boulder
345 UCB
Boulder, CO 80305

Email: tor.wager@colorado.edu
Telephone: (303) 492-7487

Table of Contents

Materials and Methods

Overview

Biomarkers were tested on four separate studies:

Study 1 served as a “training set” for the biomarker. It involved the application of noxious thermal heat at temperatures calibrated to elicit ratings of non-painful warmth, low pain, medium pain, and high pain. Participants rated pain on every trial using a visual analogue scale.

Study 2 examined whether the biomarker trained on Study 1 predicts pain in the noxious range in new individuals from a new sample. In this study we again applied heat of varying temperatures, and participants made two ratings on each trial: 1) Whether the heat was warm or painful; and 2) How intense the stimulation was.

Study 3 provided a test of *biomarker specificity*. We examined physical pain processing and responses to social pain in participants who felt rejected after a recent a romantic breakup. Participants in this experiment received non-painful and high pain stimulation and made judgments about the pain on every trial. These participants also saw pictures of their ex-partners and close friends, which comprised the Social Pain contrast.

Study 4 examined the biomarker’s ability to discriminate painful from warm stimuli in a clinicall-relevant treatment context. It tested whether the biomarker responds to treatment with remifentanil, an opiate known to have analgesic effects. Participants received high and low thermal pain trials before, during, and after remifentanil was infused intraveneously.

In this Supplement, we present methodological details of data acquisition and analysis common across the four experiments (“General Methods”), followed by details unique to each individual experiment.

General Methods

Participants

All participants provided written informed consent. Studies were individually approved by the Columbia University Institutional Review Board. For all four studies, preliminary eligibility was assessed with a general health questionnaire, a pain safety screening form, and an fMRI safety screening form. Participants reported no history of psychiatric, neurological, or pain disorders. Ethnicity was assessed using self-report screening instruments prior to study procedures.

Thermal Stimulation and Pain Rating

In all four studies, thermal stimulation was delivered to the volar surface of the left (non-dominant) inner forearm applied using a TSA-II Neurosensory Analyzer (Medoc Ltd., Chapel Hill, NC) with a 16 mm Peltier thermode end-plate. Each stimulus lasted 8-12 seconds, depending on the Study, and always included a period of time during which the stimulus ramped up from baseline temperature [32°C] to the target temperature, and another steady ramp to baseline. The ramping was intended to help prevent head movement, and analyses described below confirmed that head movement does not increase at pain onset or during pain, and does not increase with increasing temperature (Supplementary Figure S1).

Before testing in Studies 1, 3, and 4, we performed a pain calibration procedure using methods described in previous work [1,2]._In brief, we tested different sites on the forearm during calibration and used an adaptive staircase procedure to identify sites on the forearm with similar nociceptive profiles and to derive the individual participant's dose-response curve for the relationship between applied thermal stimulation and reported pain (slope, intercept, R^2). In Study 2, all participants received the same temperatures.

General fMRI Processing

FMRI data for all three studies were subjected to a standard series of preprocessing and analysis steps, which are shown in Supplementary Figure S2. The stages consisted of Preprocessing, Analysis, and Prediction/Evaluation. Preprocessing included a sequence of commonly used procedures performed using SPM software (Wellcome Trust Centre for Neuroimaging, London, UK). SPM5 was used for Studies 1, 3, and 4. SPM8 was used for Study 2, but the algorithms for all the steps we used were identical in both versions. Preprocessing also included several quality control procedures not typically performed in SPM per se, which were designed to be simple to implement (code can be obtained from wagerlab.colorado.edu or from the authors). Analysis consisted of a standard General Linear Model (GLM) analysis of each individual participant's data, and was conducted to summarize activity maps for painful heat and other conditions. Prediction involved estimating the biomarker response by computing the cross-product of these individual subject activation maps with a machine-learning biomarker pattern derived from other individuals. Specifically, the biomarker was derived from cross-validated machine learning analyses in Study 1 (see Biomarker Development below). It was applied to out-of-training-sample individual activity maps in Study 1 and new individual activity maps in Studies 2 and 3 to generate biomarker response values for each condition within each individual, which reflect a quantitative match to the pain biomarker pattern. Finally, evaluation involved quantifying the sensitivity and specificity of biomarker response to physical pain, and assessing the magnitude and significance of the opiate effect in Study 4.

These steps were employed for all analyses for all studies, except as noted below. Specifically, the initial Biomarker Development analyses involved several minor differences intended to ensure minimal artifacts in the data and minimize assumptions about the shape of the hemodynamic response to pain.

Preprocessing

Structural T1-weighted images were subjected to the following steps (Figure S2):
Coregistration (SPM). We used SPM's iterative mutual information-based algorithm to coregister volumes to the mean functional image for each subject. Coregistration was manually checked by a trained analyst, and the starting point was adjusted and the algorithm re-run until the coregistration was satisfactory.
Warping to normative atlas (SPM). Structural images were normalized to MNI space using the generative Segmentation/Warping algorithm[3] using the default parameters (7 x 8 x 7 nonlinear basis functions) and resliced to standard 2 x 2 x 2 mm voxels. Data were resampled to 3 x 3 x 3 mm voxels before biomarker development analyses (to facilitate efficient storage and processing) and before calculating biomarker response in all studies.

Functional images were subjected to the following steps (Supplementary Figure S2):

Outlier / gradient artifact detection (custom code). The purpose of this was to remove intermittent gradient and severe motion-related artifacts that are present to some degree in all fMRI data. On each individual scanning run, we identified image-wise outliers by computing both the mean and the standard deviation (across voxels) of values for each image for all slices. Mahalanobis distances for the matrix of slice-wise mean and standard deviation values (concatenated) x functional volumes (time) were computed, and any values with a significant χ^2 value (corrected for multiple comparisons based on the more stringent of either false discovery rate or Bonferroni methods) were considered outliers (less than 1% of images were outliers). For each voxel, outlier time points were imputed with the voxel's overall run mean. Next, data across the entire run were Windsorized to three standard deviations. This procedure is similar to those commonly employed by many groups (e.g., http://www.nitrc.org/projects/art_repair/).

Slice-acquisition-timing correction (SPM). This interpolates the data to correct for differences in the acquisition time for each slice.

Image realignment (SPM). This is a rigid-body (6-parameter) registration to the mean functional image, and helps correct for head movement during scanning.

Percent signal change conversion (custom code). Time series data for each voxel were converted to percent signal change based on a spatially smoothed baseline time series (16 mm FWHM).

Warping to normative atlas (SPM). Warping parameters estimated from coregistered, high-resolution structural images were applied, and functional images were interpolated to 2 x 2 x 2 mm voxels.

Analysis

Except for machine learning analyses (see Biomarker Development below), activity maps for each condition within each participant were estimated using the GLM. For each individual, a set of regressors was constructed for conditions of interest (e.g., heat at a particular temperature, aversive image presentation, etc.) using a stimulation epoch that lasted the duration of the event convolved with the canonical hemodynamic response implemented in SPM. The parameter estimates (regression slopes) for each condition thus provided an estimate at each voxel of the activation intensity for that condition. We also included a set of nuisance covariates designed to capture noise. These included, for each run: a) a constant term (intercept) for that run; b) dummy regressors for estimated outlier images from preprocessing, which varied in number depending on how many outliers were detected but was nearly always < 1% of images; and c) 24 movement-related covariates based on estimated movement during realignment, including 6 mean-centered motion parameter estimates, their squared values, their successive differences, and squared successive differences. Previous work has shown this to be helpful in reducing noise variance, violations of normality, and autocorrelation[4].

Prediction and Evaluation

All assessments of performance were made at the level of the individual subjects, always based on a biomarker developed in other individuals using cross validation (Study 1) or simply applying the biomarker developed in Study 1 to new studies (Studies 2 and 3). For all tests, the biomarker response (BR) was estimated for each test subject in each test condition by taking the dot product of vectorized activation images ($\vec{\beta}_{map}$) with the biomarker pattern $\vec{w}_{map}$, i.e., ($BR = \vec{\beta}^{T}_{map}\vec{w}_{map}$), yielding a continuous scalar value. This value depends on the voxel size, but can be scaled based on the voxel volume (see Supplementary Discussion for additional scaling considerations). Values reported in this paper are for 27 mm^3 voxels (i.e., 3 x 3 x 3 voxels). BR values derived from maps resliced to 2 x 2 x 2 mm voxels can be put on the same scale by multiplying by 27/8. We summarized the performance of the biomarker response in two ways: First, we assessed average prediction error (PE, the mean absolute deviation of predicted from observed pain ratings) when predicting continuous pain ratings. Second, we calculated sensitivity, specificity, positive predictive value, and effect sizes related to binary classification. We assessed binary classification decisions for painful stimulation relative to non-painful warmth, pain anticipation, pain recall, and social pain-inducing events.

We performed two kinds of binary classification tests. In the pain/no-pain test, sensitivity is the probability of a positive test—i.e., that the biomarker response was above a given criterion threshold—given that a person experienced pain (vs. one of the comparison conditions below). Specificity is the probability of a negative test given that a person experienced a condition other than pain. Positive predictive value is the probability that pain (vs. a comparison condition) was experienced given a positive test result. Effect size provides a continuous measure of the ability of the biomarker to separate pain from a comparison condition, and is reported as both (1) d_a, a measure of the distance between the mean biomarker response in the pain-present vs. pain-absent conditions, divided by their pooled standard deviation, and (2) the area under the Receiver Operating Characteristic (ROC) curve (AUC), estimated directly using numerical integration of the ROC under all threshold values that yielded unique sensitivity/specificity values (0.5 is chance, and 1 is perfect discrimination). In the forced-choice discrimination test, biomarker response is compared for two conditions tested within the same individual, and the higher is chosen as more painful. In the forced-choice test, the ROC curves are symmetrical, and sensitivity, specificity, and positive predictive value are equivalent to each other and to decision accuracy (i.e., the probability with which the more painful of the two conditions is selected).

The forced-choice test has several advantages that make it particularly useful in the fMRI setting. First, the forced-choice test is 'threshold free' in the sense that an absolute decision threshold across individuals is not required; zero is used as the threshold for the difference between the two paired alternatives. Thus, individual differences in the shape and amplitude of the blood oxygen level dependent (BOLD) fMRI response [5,6] do not add noise in this kind of test. In addition, as the amplitude of the BOLD response varies as a function of field strength and scanner noise, the threshold in the pain/no-pain test must be calibrated for different scanners and field strengths (see, e.g., the thresholds for Study 1, collected at 1.5 T, vs. Study 2, collected at 3.0 T, in Table 1 in the main text). Second, the forced-choice test likely provides a more realistic assessment of the biomarker's performance for validation purposes. Prediction error and sensitivity/specificity in the tests is calculated assuming that pain reports always accurately reflect experienced pain intensity in the normative samples we test here (i.e., a person reporting a "5" on the visual analogue scale always experiences more pain than a person reporting a "4"). However, this may not always be the case. Individuals may use the rating scale in somewhat different ways (e.g., the same experience may be reported by one person as a "5" on the visual analogue scale and by another as a "4"), which can reduce the apparent performance of even a perfect diagnostic test. Forced-choice discrimination performance does not require this assumption, as two conditions are compared within the same individual. The only condition that must hold for the 'ground truth' to be accurate is that an individual's pain reports must increase monotonically with pain experience; more pain should be reported as more painful.

Study 1

Participants

Twenty healthy, right-handed participants completed the study (M_{age} = 28.8 years, 8 female). The sample consisted of 79% Caucasian, 5% Hispanic, and 16% African American participants. Data were collected between 2005-2006.

Materials and Procedures

fMRI task design

fMRI images were acquired during 8 functional runs (8 trials/run, 64 trials). The thermode was placed on a different skin site for each run, with two total runs per skin site, and 12 trials at each of 4 target pain intensities—non-painful warmth (Level 1), low pain (Level 3), medium pain (Level 5), and high pain (Level 7)—were delivered across the runs. Temperatures were selected for each individual based on a thermal pain calibration procedure (see above, "Thermal stimulation and pain ratings"). At the start of each trial, a square appeared in the center of the screen for 50 ms, followed by the presentation of a cue. The cue consisted of a male or female face showing a happy or fearful expression (33 ms) followed by a mask consisting of the same face presented for 1467 ms. Participants were not aware of the type of emotional face presented, and all analyses collapse across the different face types to examine brain activity as a function of temperature and reported pain. Effects of faces will be reported in a later manuscript.

During each trial, cues (2 sec) were followed by a six-second anticipatory interval during which a fixation cross was presented on the screen. Then, thermal stimulation was delivered at one of the four intensities, followed by a 14 sec rest interval during which participants fixated on a cross. The words "How painful?" then appeared on the screen for four seconds above a 9-point visual analogue scale (VAS), and participants rated the intensity of the stimulus using an fMRI-compatible track-ball (Resonance Technologies, Inc.) Continuous responses were recorded, with resolution equivalent to the screen resolution (approximately 600 discrete values).

fMRI Acquisition and Analysis

Image acquisition. Whole-brain fMRI data were acquired on a 1.5T GE Signa Twin Speed Excite HD scanner (GE Medical Systems) at Columbia University's Program for Imaging in Cognitive Science (PICS). Structural images were acquired using high-resolution T1 spoiled gradient recall images (SPGR) for anatomical localization and warping to a standard space. Functional images were acquired with an echo-planar imaging sequence (EPI; TR = 2000 ms, TE = 34 ms, field of view = 224 mm, 64x64 matrix, 3.5 x 3.5 x 4.0 mm voxels, 29 slices), and were resliced to 3 x 3 x 3 mm voxels after inter-subject normalization. Each run lasted 6 minutes and

18 seconds (189 TRs). Stimulus presentation and behavioral data acquisition were controlled using E-Prime software (PST Inc.).

Preprocessing. Preprocessing was identical to that described in the General Methods, except that a) an additional denoising step was used to minimize artifacts for biomarker development, and b) FSL software was used for realignment. Denoising used a component-based strategy similar to published work [7,8]. We estimated the first 10 principal components (PCs) on the images from each scanning run, before any other processing. We constructed a task-related design matrix with the trail onsets convolved with the canonical HRF (no temperature information was entered to avoid bias), and a nuisance-related design matrix based on head movement parameters and outlier time points identified as described above. Components that appeared clearly artifactual (e.g., those expressed only at the edge of the brain, those that included an obvious single spike, etc.) and were related to the nuisance regressors but not the task, were removed (1.06 ± 0.59 (S.D.) components per run. Analyses of Studies 2 and 3 did not involve this step, and future studies are needed to assess the benefits of this manual procedure.

Biomarker development analysis. Biomarker development analyses were conducted on Study 1 using custom Matlab code (see 14) implementing LASSO-PCR, a cross-validated, regularized regression procedure. LASSO, or Least Absolute Shrinkage and Selection Operator-regularized regression [9], was implemented in Matlab by Guilherme Rocha and Peng Zhao. This was embedded within a leave-one-subject out cross-validation loop that first used principal components-based data reduction so that selection was performed on components, as described in previous work [10]. The resulting pattern of regression weights constituted the biomarker, which was applied to average pain maps and general linear model-based activation maps in Studies 1-3. All predictions made for Study 1 data were cross-validated (see below).

The biomarker development analysis consisted of five steps: 1) Feature selection: Voxels within an a priori mask of pain-related brain regions was selected based on prior literature; 2) Data averaging: Data during pain from each in-mask voxel were averaged within each stimulus intensity for each individual, to generate 4 pain-related activation maps per individual; 3) Machine learning: LASSO-PCR was run using those maps to predict pain reports; 4) Bootstrapping was used provide P-values for voxel weights in order to threshold the biomarker weights for display and interpretation; and 5) Permutation tests were used to validate the unbiased nature of the procedure.

1. Feature selection. To accomplish Step (1), the automated meta-analysis toolbox Neurosynth (www.neurosynth.org) was used to a create a mask based on a meta-analysis of previous studies that frequently use the word 'pain' to select voxels a priori [11]. The mask (see Figure S3A, top) was based on regions showing consistent results across 224 published studies (out of 4,393 total studies in the database) in a 'reverse inference' analysis, which was a χ^2 analysis of the 2 x 2 contingency table of counts of [activated (within 10 mm) vs. non-activated] x [pain vs. non-pain] within each voxel. Studies were counted as involving 'pain' if they mentioned 'pain' more than 1 time per 1000 words in the study (the default value in neurosynth) and thresholded at $q < 0.05$ False Discovery Rate ($P < 0.0072$) corrected. The mask included 22,379 positive voxels (2 x 2 x 2 mm, resliced to 3 x 3 x 3 mm for analysis) in which activity positively predicted pain (6.35% of the volume of the standard SPM5/8 brain mask brainmask.nii) and 10,940 negative voxels in which activity negatively predicted pain (3.1%), for a total of 9.45% of the in-brain volume. Weights from all voxels in this mask were used to estimate biomarker response and make predictions (no further thresholding was used for predictive purposes).

2. Data averaging. To accomplish Step (2), we averaging data within each trial in each voxel over the period 8-24 seconds after heat onset, and then averaged across the 12 trials for each stimulus intensity. This time window was chosen a priori based on the approximate time when reported pain is high from previous work [12-15]; which is later than typical responses for a similar stimulation epoch due to temporal summation and hemodynamic lag in pain-related activity [13,16]. Simple averaging has the advantage of simplicity and lack of strong assumptions about the shape of the hemodynamic response, although improvements in the use of timing information is a rich direction for future improvement that has already started to be explored [17].

3. Machine learning. To accomplish Step (3), we used cross-validated LASSO-PCR with activation maps from each condition within participants as the predictor, and average pain reports from each condition within participants as the outcome. The linear algorithm provided interpretable brain maps [10,18] composed of linear weights on voxels, which is a substantial advantage over nonlinear kernel methods. We did not explore nonlinear methods here.

We used leave-one-subject-out cross-validation to estimate prediction error (PE; mean absolute deviations between predicted and actual temperatures) on new trials. This standard approach in machine learning involves dividing the sample into a training set (all but one participant) and a test set (the test participant). LASSO-PCR was used to estimate regression weights for each voxel from the training dataset ($\vec{w}_{map}$, the biomarker pattern), and then predictions were made for the test participant by and taking the dot-product of the test brain activation maps ($\vec{\beta}_{map}$) and the biomarker pattern ($\vec{\beta}_{map} \bullet \vec{w}_{map}$). This yielded a scalar predicted pain value (the biomarker response) for each condition, and prediction error was quantified. The procedure was repeated 20 times (once for each participant) so that each trial was part of the test set exactly once. This procedure yields minimally biased estimates of prediction accuracy for new participants (there is a slight bias in accuracy towards zero, as with all cross-validation methods). Weight maps applied to Study 1 were always based on data from out-of-test-sample individuals, and the final biomarker weights (applied to Studies 2-4) were based on the full Study 1 sample.

To apply the biomarker to new activation maps across multiple conditions (i.e., anticipation, stimulation, and pain recall at each intensity, and other maps in Studies 2-4), we used a standard general linear model (GLM) with the canonical SPM hemodynamic response function to simultaneously estimate activation maps ($\vec{\beta}_{map}$) for each condition, and then applied the biomarker pattern ($\vec{\beta}_{map} \bullet \vec{w}_{map}$) to yield a scalar biomarker response value for each condition. The biomarker response values are thus predictions of the magnitude of pain for a given condition, and their values across conditions can be compared and tested.

In our initial analyses of Study 1, we compared LASSO-PCR results with those from another popular method, Support Vector Regression (SVR; [19]) in order to check whether predictions were similar and whether SVR produced similar accuracy levels. Predictions and accuracy levels were nearly identical with SVR in all cases (predictions between LASSO-PCR and SVR were correlated > r = 0.99 in most cases), so we do not focus on the SVR results. We prefer the LASSO-PCR results for transparency and consistency with our previous work. LASSO-PCR and SVR produced very similar results in all analyses we performed, and we do not consider the choice of algorithm to be critical, though algorithms that yield improved results could be developed.

*4. Bootstrap tests***.** To accomplish Step (4) and threshold voxel weights for interpretation and display, we constructed 5,000 bootstrap samples (with replacement) consisting of paired brain and outcome data and ran LASSO-PCR on each. Two-tailed, uncorrected P-values were calculated for each voxel based on the proportion of weights below or above zero, as in previous work (1, 20), and subjected to False Discovery Rate correction ($P < 0.0028$, 355 significant voxels; Supplementary Figure S3B, C). The biomarker weight map applied to Studies 1-3 for diagnostic purposes was not thresholded; all weights were used.

5. Permutation tests. To accomplish Step (5), we permuted the data 5,000 times, repeating the cross-validated LASSO-PCR analysis for each permuted dataset. The correlation between predicted and observed pain should be symmetrically distributed around zero if the procedure is unbiased, and this was tested and confirmed (Supplementary Figure S3D). In addition, the mean prediction error and predicted pain-observed pain correlation were far lower and higher, respectively, for the correct permutation ($P < 0.001$ for both; Figure S3D), demonstrating that the prediction results were far better than what would be expected by chance.

Study 2

Participants

Thirty-three healthy, right-handed participants completed the study ($M_{age} = 27.9 \pm 9.0$ years, 22 females). The sample consisted of 39% Caucasian, 33% Asian, 12% Hispanic, and 15% African American participants. Data were collected between 2010-2011.

Materials and Procedures

Thermal stimulation and pain ratings

Thermal stimulation was delivered to locations on the left volar forearm that alternated between runs. Each stimulus lasted 12.5 seconds, with 3-second ramp-up and 2-second ramp-down periods and 7.5 seconds at target temperature. Trials at six discrete temperatures were administered (level 1: 44.3°C, level 2: 45.3°C, level 3: 46.3°C, level 4: 47.3°C, level 5: 48.3°C, level 6: 49.3°C). After each stimulus, participants rated explicitly whether it was painful or not. If they rated it as non-painful, they were then prompted to rate warmth intensity on a 100-point VAS anchored with "no sensation at all" and "very warm but not yet painful." If they rated it as painful, they rated pain intensity on a 100-point VAS anchored with "no pain" and "worst imaginable pain."

fMRI task design

FMRI images were acquired during 10 functional runs. Runs 1, 2, 4, 8 and 9 were "standard" runs, during which were delivered a total of 11 stimulations from each of levels 1-5, for a total of 55 stimuli. Transitional frequencies were counterbalanced so that each temperature was preceded twice by each of the five temperatures and each run started with a different temperature. Different presentation orders were generated for each participant. On Runs 5-6 temperatures were increased one degree, with 4 stimuli at each of levels 2-6. During two additional runs (not analyzed here), participants were instructed on the use of mental imagery to modify pain. These are beyond the scope of the current paper and will be presented elsewhere.

Each trial consisted of a stimulus (12.5 sec), a 4.5-8.5 sec delay, a 4 sec painful/non-painful decision period (participants pressed the left or right button on the side of an MR-compatible trackball), a 7-sec continuous warmth or pain rating period (VAS ratings were made using the trackball and confirmed with a button-press), and 23-27 sec of rest. During both rest and stimuluation, participants fixated on a cross presented on-screen.

fMRI Acquisition and Analysis

Imaging acquisition. Whole-brain fMRI data were acquired on a 3T Philips Achieva TX scanner at the PICS Center. Structural images were acquired using high-resolution T1 spoiled gradient recall images (SPGR) for anatomical localization and warping to a standard space. Functional EPI images were acquired with TR = 2000 ms, TE = 20 ms, field of view = 224 mm, 64x64 matrix, 3 x 3 x 3 mm voxels, 42 interleaved slices, parallel imaging, SENSE factor 1.5. Runs lasted between 6:22 and 6:58 (191 or 209 TRs). Stimulus presentation and data acquisition were controlled using E-Prime.

Preprocessing and analysis. Image preprocessing and analysis were performed as described under General fMRI Processing above. First-level GLM analyses for each participant included regressors for stimulation periods for each of the 6 levels and the 11-sec rating periods, linear drift across time within each run, and indicator vectors for outliers and head movement as described above. The biomarker pattern from Study 1 was used to estimate the biomarker response for each participant in each condition, and these values were used in binary classification analyses.

To assess classification performance for painful vs. non-painful trials, we averaged biomarker responses for non-painful and painful trials, and subjected these average responses to sensitivity/specificity analyses. Because this study was collected on a different scanner with a higher field strength, biomarker responses were on a different scale and a different classification threshold was determined for pain/no-pain classification. Forced-choice analyses are threshold-free and do not require this adjustment.

Regression models. In a second model, we included separate regressors for each individual trial, and applied the biomarker pattern from Study 1 to estimate the biomarker response for each individual trial. We used these values in mixed effects regression models predicting pain and temperature. Both warmth ratings and pain ratings were very sensitive to temperature increases: Pain ratings increased 20.8 ± 12.9 (SD) units/°C, and warmth ratings increased 17.7 ± 12.7 units/°C.

In the regression analyses, we tested models in which we assessed performance in predicting pain controlling for temperature. To completely control for temperature, we included covariates that controlled for all possible pairwise differences between temperatures (level 6 vs. 5, 5 vs. 4, 4 vs. 3, 3 vs. 2, and 2 vs. 1), thus controlling for temperature estimated in a nonparametric fashion, without assuming linearity. This analysis removed much of the variation in pain report (as most of the variance was caused by temperature), but served as a test of whether biomarker responses predicted pain even when completely accounting for the effects of heat itself.

Study 3

Participants

Forty right handed, native English speakers (21 females, M_{age} 20.78, SD = 2.59) gave informed consent. All participants experienced an unwanted romantic relationship break-up within the past six months (M = 2.74 months; SD = 1.70 months), and indicated that thinking about their break-up experience led them to feel rejected. All participants scored above the midpoint on a 1 (not at all rejected) to 7 (very rejected) scale that asked them to rate how rejected they feel when they think about their rejection experience (M = 5.60, SD = 1.06). The sample consisted of 60% Caucasian, 20% Asians, 10% African Americans, and 10% other ethnicities. Data were collected between 2007-2008. Data on the basic group activation maps for physical and social pain contrasts were published previously[20], but the analyses and substantive conclusions were different from and complementary to those reported here.

Materials and Procedures

Social Pain Stimuli

The social rejection task was modeled after (a) fMRI research that used photographs provided by participants to elicit powerful emotions, including maternal love, romantic love, and rejection (21-24) and (b) behavioral research indicating that cueing people to recall autobiographical rejection experiences is an effective way of reactivating social rejection related distress (e.g., 25, 26, 27). The stimuli for this task consisted of: (a) a headshot photograph of each participant's ex-partner and a same gendered friend with whom they shared a positive experience around the time of their break-up (M = 2.46 months; SD = 1.70 months), and (b) cue phrases appearing beneath each photograph which directed participants to focus on a specific experience they shared with each person.

All photographs were cropped so that the total area of the photograph taken up by the face was constant across ex-partner and friend images (t = 1.42, P = .16). To be sure that the photographs participants provided were matched in terms of picture quality, we had a group of ten individuals who were blind to the study goals and hypotheses rate the picture quality of each photograph. Ex-partner and friend photographs did not differ significantly on this dimension (t = 1.32, P = .20). Judges also rated the attractiveness level of the individuals depicted in ex-partner and friend photos, which also did not differ significantly (t = .89, P = .38).

When participants viewed the photograph of their ex-partner during the social rejection task they were instructed to think about how they felt during their specific break-up experience; when they viewed the photograph of their friend they were instructed to think about how they felt during their recent positive experience with that person. To help participants focus on these specific experiences during the task we included a short cue phrase beneath each photograph (e.g., "rejected by Marc"; "party with Ted"). Participants generated these cue phrases on their own, prior to the day of scanning using a procedure developed in prior research [21]. Specifically, they first wrote about their specific break-up experience with their ex-partner and their specific positive experience with their friend. Subsequently, they were asked to create a cue phrase that captured the gist of their experience. They were reminded of the cues they generated and their break-up experiences on the day of scanning following established procedures [21].

Physical Pain Stimuli

As in Study 1 and prior research [2,14,22], a calibration procedure was used to select heat intensities that participants judged to be non-painful ("warm," Level 2 on a 10-point scale) vs. near the limit of pain tolerance ("hot," as close as possible to Level 8 on a 10-point scale, though intensity was capped at 48°C). The mean low temperature for the sample was 39.9°C (SD = 2.76°C); the mean high temperature was 46.6°C (SD = 1.72°C). In the scanner, participants rated both physical and social pain on a 5-point scale using a five-button unit under their right hand, with lower numbers reflecting more distress.

Task Training

Prior to scanning, the experimenter walked participants through each step of the social rejection task (referred to as the "photograph" task to participants) and the physical pain task (referred to as the "heat" task to participants). They were told that that during the "photograph" task they would see the photographs of their ex-partner and friend. The experimenter explained that beneath each photograph the cue-phrases they generated earlier would appear. When they saw each photograph they were asked to look directly at it and think about how they felt during the specific experience associated with the cue-phrase. Thus when participants viewed the photograph of their ex-partner they were directed to think about how they felt during their break-up experience with that person; when they viewed the photograph of their friend they were directed to think about how they felt during their positive experience with that person. During the physical pain task, participants were instructed to focus on the fixation cross that appeared on the screen during the trials, and think about the sensations they experienced as the thermode on their arm heated up. They were then instructed how to rate their affect after each type of trial, and how to perform the visuospatial control task.

fMRI Acquisition and Analysis

Acquisition

Whole-brain functional data were acquired on a GE 1.5 T scanner at the PICS Center (the same scanner used in Study 1) in 24 contiguous axial slices (4.5 mm thick, 3.5 x 3.5 mm in-plane resolution) parallel to the anterior commissure-posterior commissure (AC- PC) line with a T2*-weighted spiral in out sequence (repetition time [TR] = 2000, echo time [TE] = 40, flip angle = 84, field of view [FOV] = 22.4) in 4 runs of 184 volumes each (368 sec each). Structural data were acquired with a T1-weighted spoiled gradient recalled echo scan (180 slices, 1 mm thick, in-plane resolution 1 x 1 mm; TR = 19,TE = 5, flip angle = 20, FOV = 25.6).

Analysis

Image preprocessing and analysis were performed as described under General fMRI

Processing above, except that functional data were smoothed with a 6 mm FWHM Gaussian kernel after spatial warping and prior to analysis (as done in a prior publication on these data; [20]). First-level GLM analyses for each participant included regressors for Rejector photos, Friend photos, Hot (painful) stimulation, and Warm (peri-pain threshold) stimulation periods, as well as covariates for the 5 sec affect rating periods for each condition and movement and outlier covariates for each run. The biomarker pattern from Study 1 was used to estimate the biomarker response for each participant in each condition, and these values were used in binary classification analyses.

Study 4

Participants

Twenty-one healthy, right-handed participants completed the study (M_{age} = 24.7 ± 4.18 years, 11 females). The sample consisted of 40% Caucasian, 15 % Asian, 30% Hispanic, and 15% African American participants. Data were collected between 2007-2008. Data on dissociable drug effects and expectancy effects were published previously[23], but the analyses and substantive conclusions were different from and complementary to those reported here.

Materials and Procedures

Thermal stimulation and pain ratings

FMRI images were acquired during 2 functional runs of 6 blocks each (6 trials/block, 64 trials), with 30-second breaks between blocks, during which an experimenter rotated the thermode location. The thermode was placed on a different skin site for each block, and skin sites were stimulated in the same order on each run. Temperatures were selected for each individual based on a thermal pain calibration procedure (see above, “Thermal stimulation and pain ratings”), and thermal stimulation alternated between stimuli calibrated to elicit low pain (Level 2; *M* = 41.16°C, SD = 2.64) and high pain (level 8; *M* = 47.05°C, SD = 1.69).

Remifentanil administration and experimental design

During fMRI scanning, participants received remifentanil hydrochloride (Ultiva; Mylan Institutional) intraveneously under two conditions: Open administration, in which participants were fully informed about the drug infusion, and Hidden administration, during which participants were told they would receive no drug. Remifentanil administration proceeded identically in both runs. Participants received remifentanil at doses individually selected to elicit pain relief without sedation, based on a pre-experiment dosing procedure. The average dose administered was 0.043 µg/kg/min (SD = 0.01). Remifentanil infusion began after the first block (before trial 7), and infusion proceeded steadily throughout blocks 2-4. A washout period began following the fourth block, and anatomical images were acquired between runs to ensure there was no remifentanil in the system at the start of the next run.

At the start of each trial, participants heard an auditory tone (an orienting cue) and saw the words "warm" or "hot" on the screen for 3 s. Following a 7-13s jittered anticipation interval (*M* = 10.16 s, SD = 2.64), participants felt heat from the thermode at temperatures calibrated to elicit either low or high pain (1.5s ramp-up, 7s at peak, 1.5s ramp-down). This was followed by a 9-15 s rest interval (*M* = 11.67 s, SD = 2.50), during which participants fixated on a cross. The words "How painful?" then appeared on the screen for 4 - 6 seconds above a 9-point visual analogue scale (VAS), accompanied by an orienting tone. As in Study 1, participants rated the intensity of the stimulus using an fMRI-compatible track-ball (Resonance Technologies, Inc.). The next trial began after 9-15s (*M* = 11.46s, SD = 2.57).

fMRI Acquisition and Analysis

Image acquisition. Whole-brain structural (T1-weighted SPGR) and EPI fMRI data were acquired on a 1.5T GE Signa Twin Speed Excite HD scanner (GE Medical Systems) at Columbia University's Program for Imaging in Cognitive Science (PICS), as in Studies 1 and 3. (EPI; TR = 2000 ms, TE = 34 ms, field of view = 224 mm, 64x64 matrix, 3.5 x 3.5 x 4.0 mm voxels, 28 slices). Each run lasted 33 minutes and 20 seconds (1000 TRs), divided into six blocks, with a brief pause between blocks 4 and 5 to prevent scanner overheating. Stimulus presentation and behavioral data acquisition were controlled using E-Prime software (PST Inc.).

Preprocessing. Preprocessing was identical to that described in the General Methods, except that FSL software was used for realignment.

Analysis. We used first-level (single-subject) GLM regression parameter estimates from our previously published study [23] (but adjusted to 3 x 3 x 3 mm voxels), which maintained consistency in modeling of the events and drug effects across the previous report and this one. Full details of the model are provided in the previous publication[23], but in brief, we modeled effects of painful (Hot) and non-painful (Warm) stimulation in each of Open and Hidden runs with separate regressors. model drug effects across time, we used a pharmacokinetic model and parameter estimates based on age, weight, and sex[24,25] to estimate the drug effect site concentration second-by-second during drug infusion. Those values were normalized to a peak amplitude of 1 and used to create a "parametric modulator" regressor for each condition, which is orthogonal to the average regressor across trials and estimates changes in heat-evoked responses across time that are linearly related to drug effect site concentration. Example regressors for Hot trials are shown in Supplementary Figure S5A. The regressor capturing the average response across trials is shown in green, and the drug concentration regressor is shown in red. To capture additional effects of expectations and other time-varying effects that do not follow the time-course of drug effects, we included an additional parametric modulator, which modeled the period of infusion vs. pre- and post-infusion baseline, orthogonalized to the drug effect site concentration regressor. This is shown in blue in Supplementary Figure S5. Together, the regressors capture a range of modulatory effects across time, including drug effects based on the pharmacokinetic model (Supplementary Figure S5B).

To test Hot vs. Warm and drug effects on the biomarker response, we applied the biomarker pattern from Study 1 to each regression parameter estimate ($\vec{\beta}_{map}$) map to yield a single amplitude value (BR) for each regressor within each participant. The significance of the drug modulation effect on biomarker response was tested by conducting a t-test on the BR values for the drug effect site concentration regressor. To visualize the responses (Figure 4, Supplementary Figure S5C), we reconstructed the fitted responses for Hot and Warm trials in each of Open and Hidden administration by multiplying the appropriate regressors in the design matrix X by BR for each participant. This yielded an overall fitted time course for each condition within each subject (averages across participants are shown in Supplementary Figure S5C). To conduct analyses on pre-drug infusion and peak drug infusion trials, we constructed a GLM design matrix with regressors for each trial, and used it to estimate the amplitude of the fitted response on each trial. Those estimates, averaged across participants, are shown by the solid line in Supplementary Figure S5C. Estimates for pre-drug infusion trials were obtained by averaging across amplitudes for Trials 1-3 for each participant, and estimates for peak drug infusion trials were obtained by averaging amplitudes for Trials 10-12.

Supplementary Results

The following analyses examine several methodological aspects of the study, and presented as supporting information. They demonstrate that a) head movement is not induced by thermal stimulation and does not drive pain-predictive results; and b) the time course of the biomarker response tracks pain experience more closely than the time course of noxious heat itself.

Head movement analyses

In Study 1, to assess whether noxious thermal stimulation caused head movement, we quantified relationships between head movement and time within trial (anticipation, stimulation, and rating periods). We estimated head movement by taking the absolute successive differences between motion estimates from rigid-body image realignment during preprocessing. For each of the six directions of potential movement (lateral, anterior-posterior, and inferior-superior translation and roll, pitch, and yaw), movement was highest at the onset of the pain-predictive cue, but was still within standard tolerances even for the worst movement direction (< 0.08 mm / 0.06 degrees; Supplementary Figure S1A/B). Movement dropped within a few seconds to low levels, and stayed low throughout the stimulation epoch without responding to heat onset or offset. We also averaged head movement during the stimulation epoch as a function of stimulus temperature. Mixed-effects regression analyses revealed no significant relationships between temperature and head movement for any parameter (Supplementary Figure S1C/D). Effect sizes ranged from Z = 0.17 - 0.92, all P > 0.10. Similar results were obtained for other studies, but are omitted here for brevity.

We also quantified the degree to which head movement and the inclusion of movement-related covariates impacted the sensitivity/specificity analyses. If pain is correlated with head movement, including head movement-related covariates should reduce performance in discriminating pain from other conditions. Conversely, if it is unrelated, controlling for head movement may increase discrimination accuracy by removing noise in the fMRI data. Across the six analyses of sensitivity/specificity reported for Study 1 (Pain vs. Low pain, Pain vs. Anticipation, and Pain vs. Pain Recall for each of pain/no-pain discrimination and forced-choice discrimination cases), effect sizes were moderately larger when controlling for head movement as described above (difference in d_a = 0.03 - 0.83, mean = 0.49). Similar results were obtained for other studies, but are omitted here for brevity.

The time course of biomarker response

To examine the time course of the biomarker response during thermal stimulation and further assess the relationship with pain vs. heat sensation across time, we reconstructed biomarker response every 2 sec during the various phases of the stimulation trials: anticipation of pain, pain experience, pain judgment, and rest (Supplementary Figure S4). Biomarker response rose during the application of heat and monotonically tracked the actual temperatures, but did not respond to anticipatory cues or post-pain decision-making periods, demonstrating specificity to the time period when pain was experienced. In addition, stimulus delivery and subjective pain follow different time courses due to temporal summation[16,26], permitting a test of which correlates more highly with biomarker response. We estimated the time course of subjective pain during heat epochs in a separate sample (N = 12), and convolved that time course with the canonical SPM hemodynamic response function to obtain a prediction based on expected moment-by-moment pain experience (purple in Fig. S4B). We contrasted that with a model in which the time course of stimulation itself was convolved with the canonical SPM hemodynamic response function to obtain a prediction based on moment-by-moment heat intensity.

We estimated the slope of the relationship between biomarker activity and temperature at each time point for each participant. Correlation between the time course of biomarker temperature effects (slopes) and predicted fMRI responses were higher for the pain report predictor than the stimulation time course for every individual tested ($r = 0.89 \pm 0.007$ vs. $r = 0.76 \pm 0.01$, respectively; $P < 0.001$; Fig. S4C). These results further suggest specificity to pain experience rather than general salience, somatic sensation, or decision processes.

Supplementary Discussion

Future directions: Expanding and improving biomarker performance

The findings reported here provide a foundation for testing hyperalgesic and allodynic responses in patient groups; testing effects of drug treatments [27,28] and psychological interventions such as placebo effects [1,29], distraction [30], and other interventions; and defining subgroups of individuals who may differ in the neurophysiological basis for pain [31,32].

A challenge that remains for future research is the substantial variability across individuals, particularly patient groups [33]. Here, the biomarker was able to predict relative pain differences in new individuals (the forced-choice test) better than absolute pain intensity across individuals (the pain/no-pain test). Forced-choice tests within individuals picked out the more painful of two conditions 90-100% of the time when those conditions differed at least moderately in the degree of pain. However, pain/no-pain classification of single images across individuals was somewhat lower (73 – 100% sensitivity and specificity, depending on the test).

This difference is likely due primarily to differences in a) session-to-session variability in scanner performance and data quality [34]; b) individual differences in usage of the ratings scales; c) individual differences in vascular response magnitude and shape [6]; d) failure of the model (linear weights) to capture critical aspects of the brain representation of pain; e) inter-individual differences in the topography of pain and the localization of the critical brain regions; and f) when using the same criterion threshold across studies, differences in the amplitude of the BOLD response depending on acquisition and analysis parameters (see below). All of these influence absolute assessments of pain across individuals, but only (d), (e), and to a lesser extent (c) are likely to influence forced-choice performance..

Each of these sources of variability suggests different routes to improving and extending biomarker development, and offer a rich variety of directions for work in future studies:

(a): Inter-session variability and noise can be improved by higher-field imaging, better control and modeling of physiological noise, and better calibration within and across scanners [35]. Improved detection and mitigation of artifacts is also important, and quality-control metrics that can establish when fMRI data should not be trusted are critical for clinical use.

(b): Individual differences in rating scale usage will increase error in even a hypothetically perfect, noise-free biomarker. These present an ongoing problem for biomarker validation, but one of the advantages of having an objective biomarker is that it can be used as a benchmark for improving rating scales (and vice versa.)

(c): Individual differences in vascular response properties can be mistaken for differences in pain-related signals, as they influence fMRI response magnitude and model fit. This type of variability can be further mitigated by 1) determining the fMRI time courses that optimally predict pain [13,17], 2) characterizing individual differences in the timing of the stimulus-pain relationship [12], and 3) calibrating the magnitude of pain-related responses across individuals [36].

(d): It is notable that a single map of linear voxel weights was able to predict pain reliably across individuals. However, it is possible that linear or non-linear interactions among brain systems contains more reliable information than the linear map we used here, and that some aspects of pain are encoded or modulated by systems outside the *a priori* brain mask we used. The use of high-resolution fMRI, non-linear algorithms, feature selection and inclusion of additional brain regions, and incorporation of functional connectivity may all improve performance [33]. The utility of these approaches is likely to emerge as data quality improves, making it possible to robustly estimate more complex models.

(e): In pain and other domains, normal variation in topography is known to make prediction across individuals based on a common brain space more difficult [37-39]. Spatial variability may be reduced by improved inter-subject registration or the use of algorithms that register brains in functional space directly [40]. It may also be possible to develop hybrid tests that make use of trusted information about an individual's pain in order to test other kinds or aspects of pain that require validation. However, different individuals and patient groups may also have fundamentally different topography in the organization of pain systems [41]. Biomarkers that explicitly test the topography of pain representations in the cortex and subcortex could be developed to characterize and understand this variability.

(f): An additional challenge for future studies concerns the equation of the absolute scale of biomarker response values across scanners and studies. Scaling issues are important when using the pain/no-pain test and attempting to use a consistent criterion threshold for classification across scanners. The calibration of BOLD fMRI across scanners and imaging acquisition and analysis choices is an active field of research (e.g., [42,43]). The amplitude (i.e., percent increase) of stimulus-evoked BOLD responses depends on field strength, TR, TE, acquired voxel size, and flip angle, on the local concentration of water in tissue. For example, Donahue et al. [42] compared intravascular and tissue BOLD signal in the same individuals at the same spatial resolution (3.5 x 3.5 x 3.5 mm, comparable to our studies) and found that signal amplitude varies log-linearly with TE and somewhat less than linearly with field strength. BOLD response amplitude also depends on the choice of baseline state, stimulus timing that may result in nonlinearity in BOLD responses, physiological noise removal and filtering choices, and the scaling of model regressors and contrast weights.

Here, all studies were conducted with approximately the same voxel size, TE (except Study 2), use of open-eyed fixation as a resting baseline, stimulus timing, and modeling, which allowed the same criterion threshold to be used across studies. Studies 1, 3, and 4 were conducted at 1.5 T and Study 2 was conducted at 3 T. Based on the results of Donahue [42] and the field strength/TE combination used in Study 2, we estimated that the response amplitude in Study 2 should be 1.355 times larger than Study 1, resulting in somewhat larger BR values. Thus, the criterion threshold used in Study 1 would correspond to a threshold of 1.897 in Study 2, which is somewhat higher than the optimal calculated threshold of 1.32 for Study 2. However, the Study 1 threshold was optimized to separate high-intensity from low-intensity stimuli, whereas the Study 2 threshold was optimized to separate painful from non-painful stimuli across a continuous range, with explicit painful/non-painful judgments on each trial. Thus, it is not surprising that the threshold is somewhat lower for Study 2. Overall, the results show substantial promise for calibration across studies, which will be aided by further research on calibrated BOLD.

Supplementary Figure S1

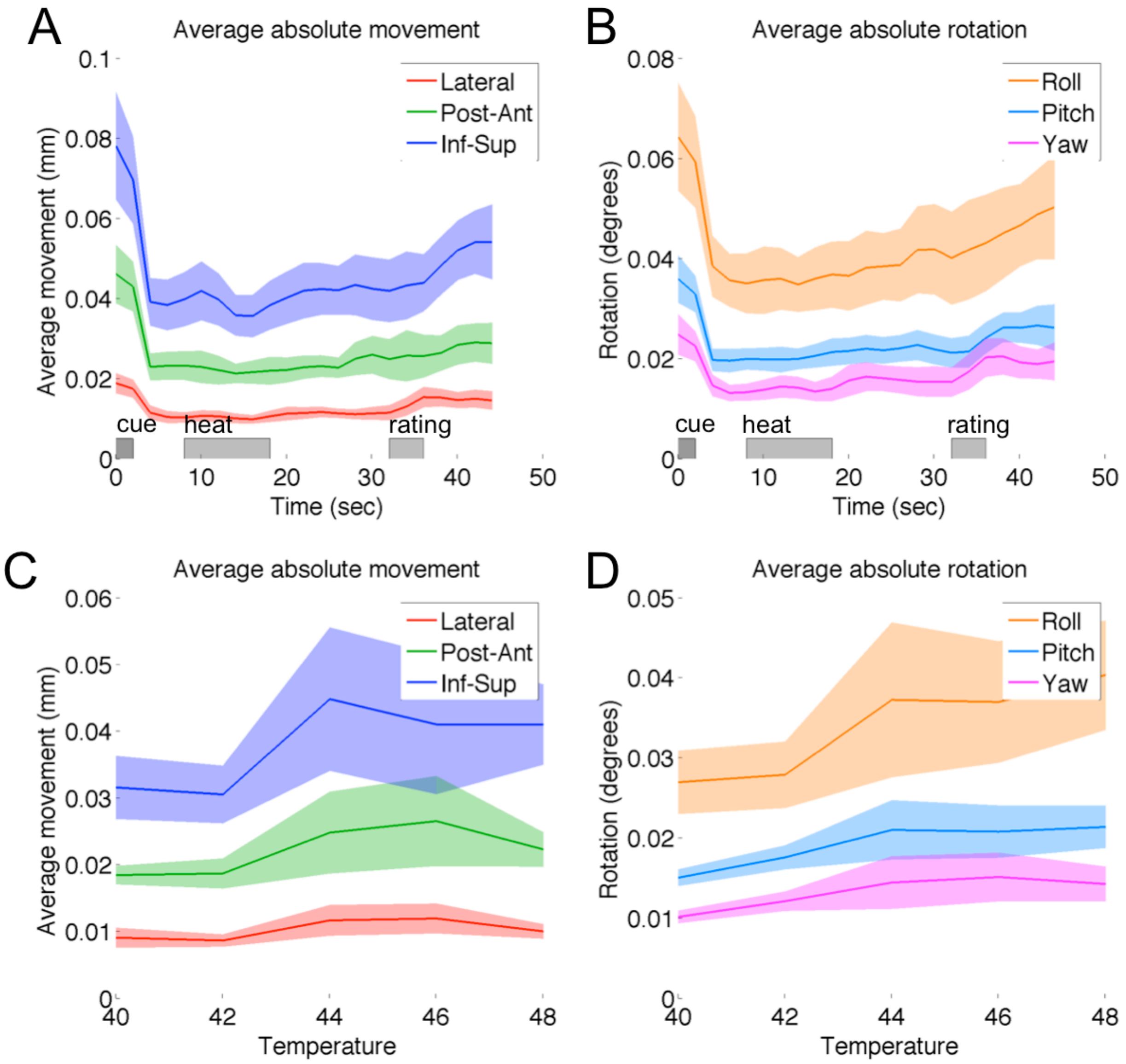

Head movement in Study 1. Three translation (A, C) and three rotation (B, D) parameter estimates, based on image realignment, are plotted as a function of time within the heat trial (A, B) and stimulus temperature (C, D). In each case, the average absolute displacement from the previous image is plotted on the y-axis. Error bars show standard error of the mean. Head movement did not increase during stimulation or at stimulus onset and offset. Rather, a modest movement increase is observed at the onset of the pain-predictive cue. Movement was not significantly predicted by temperature for any movement direction.

Supplementary Figure S2

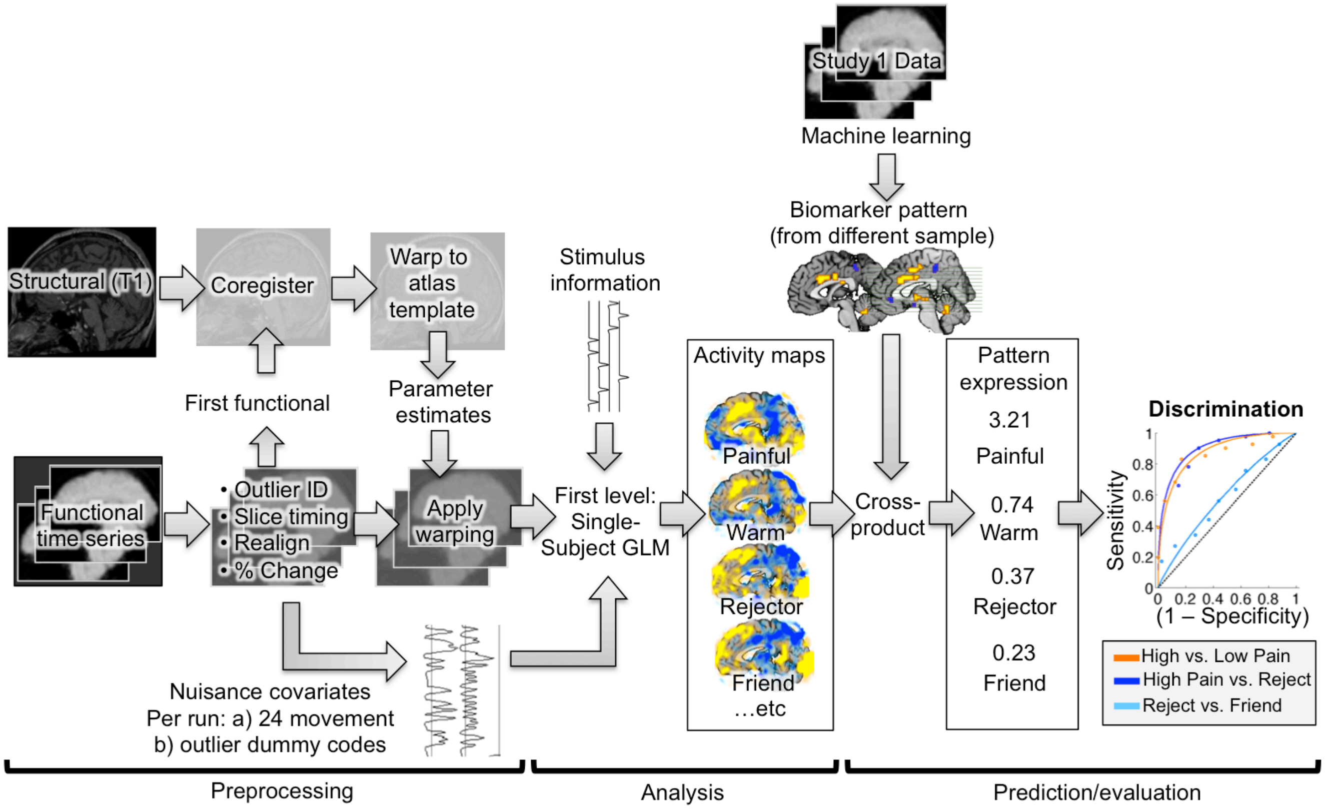

Preprocessing and analysis stages. The preprocessing and first-level General Linear Model (GLM) are standard steps performed with SPM software, with the exception of outlier identification and percent-change scaling. Activity maps from the GLM are cross-multiplied by the biomarker map, which was developed using a separate cross-validated machine learning regression (not illustrated), to yield a scalar biomarker response value for each image. Biomarker response values are used to predict continuous pain and in classification.

Supplementary Figure S3

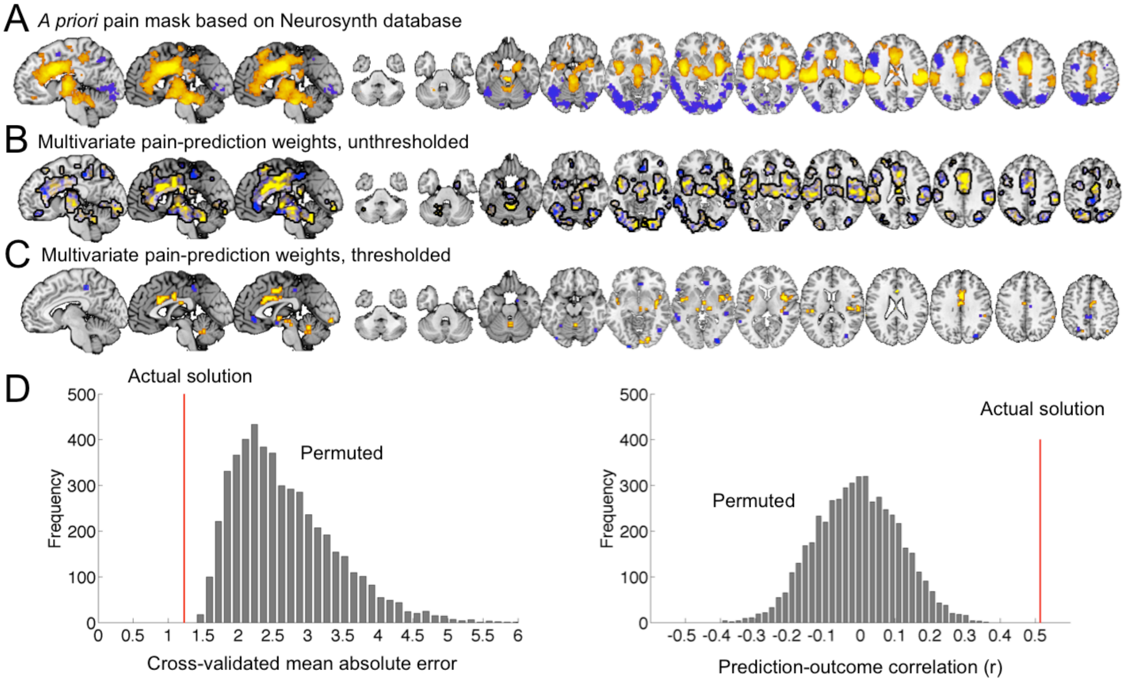
A *A priori* pain mask based on Neurosynth database
B Multivariate pain-prediction weights, unthresholded
C Multivariate pain-prediction weights, thresholded
D
Actual solution
Permuted
Frequency
500
400
300
200
100
0
0 0.5 1 1.5 2 2.5 3 3.5 4 4.5 5 5.5 6
Cross-validated mean absolute error
Actual solution
Permuted
Frequency
500
400
300
200
100
0
-0.5 -0.4 -0.3 -0.2 -0.1 0 0.1 0.2 0.3 0.4 0.5
Prediction-outcome correlation (r)

Biomarker development in Study 1. A) A mask of a priori regions used in analysis based on the Neurosynth database, associated with 'pain' at q < 0.05 FDR-corrected. In all plots, yellow indicates positive predictive weights for pain, and blue indicates negative weights. B) Unthresholded biomarker pattern weights from the LASSO-PCR analysis, shown as Z-scores, with voxels with lower Z-scores more transparent. The black outline shows the a priori mask boundaries. Blue/yellow indicate Z < -2 and Z > 2, respectively. C) Map thresholded at q < 0.05 FDR (P < 0.003) for display. Blue/yellow indicate Z < -3 and Z > 3, respectively. D) Histograms of prediction error and prediction-outcome correlation from nonparametric permutation test. Histograms show the distribution of null-hypothesis results, and the red line shows the actual solution.

Supplementary Figure S4

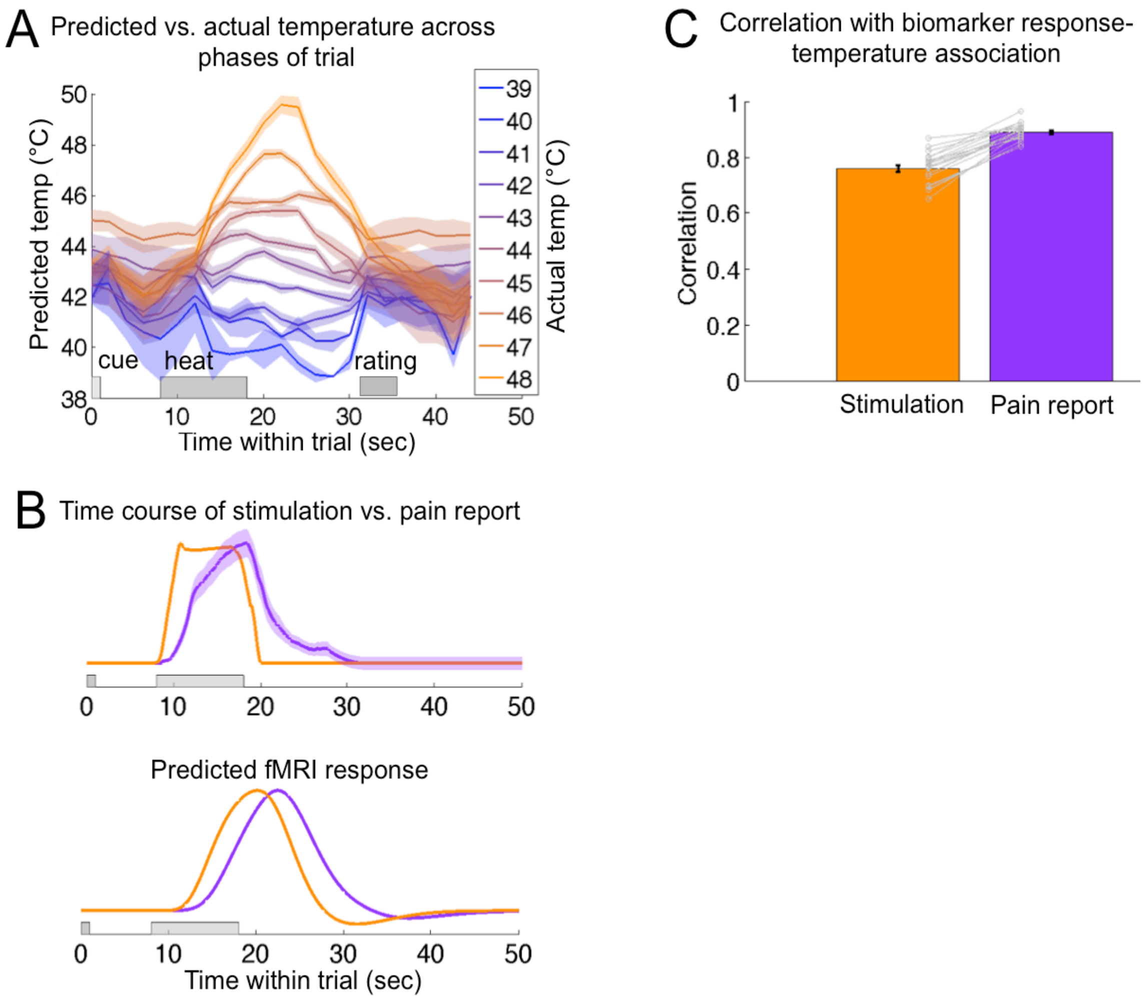

Correlation of biomarker activity with the time course of objective stimulus delivery vs. reported pain in Study 1. A) Biomarker response (scaled to reflect predicted temperature) across time within trials. Lines/shading: means/standard errors across participants. Pattern expression increased monotonically with temperature only following stimulation, and not during cue and pain report periods. B) Top: Time-course of thermal stimulation (orange) and subjective pain (purple; shaded area: SEM). Bottom: Predicted fMRI activity, convolving the stimulus and report time-courses with SPM's standard double-gamma hemodynamic response function. The predictors were correlated (r = 0.78, 61% of variance shared), but the pain time course peaked appreciably later. C) Correlation between the time course of biomarker temperature effects and the model were higher for the pain report model (purple) than the stimulation time course model (orange) for every individual tested. Correlations for individual subjects are shown by points connected with light gray lines.

Figure S5. Modeling of drug effects on biomarker response in Study 4

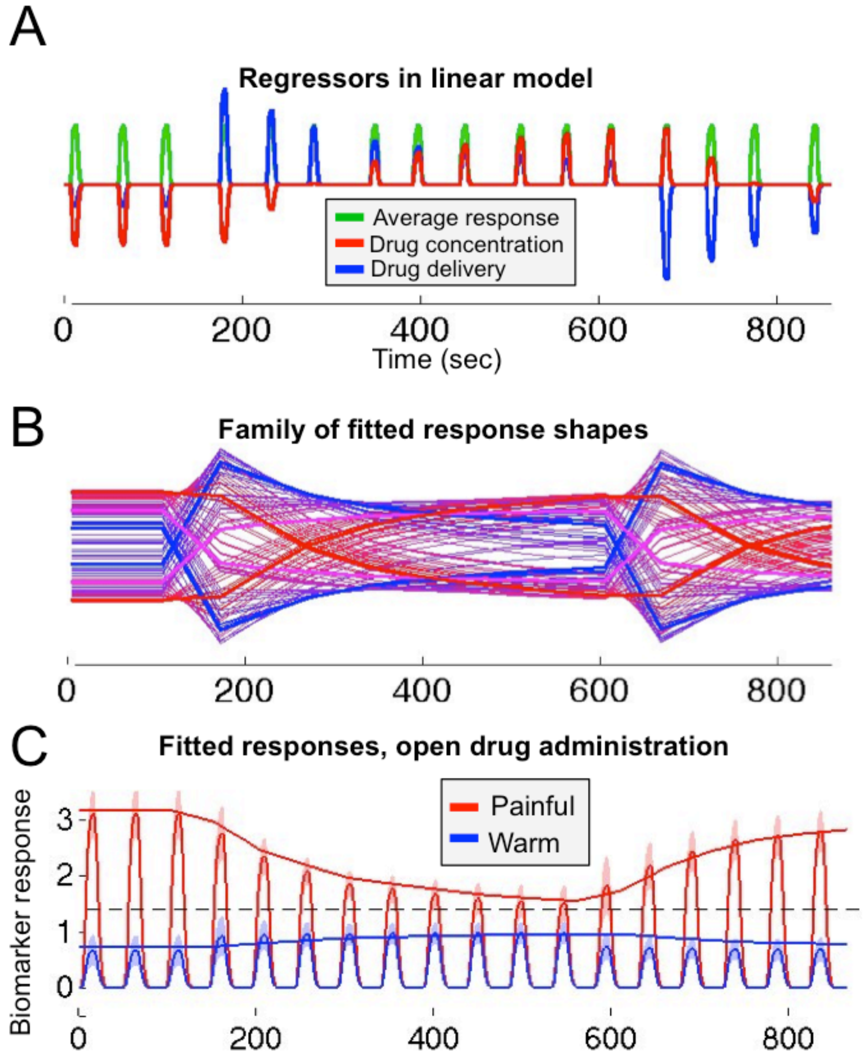

Modeling of drug effects in Study 4. A) Regressors for the average response (green), drug effect site concentration estimated using a pharmacokinetic model (red), and the drug infusion period itself, orthogonalized to the drug regressor (blue). B) The family of shapes modeled by the modulator regressors (red and blue). C) The average fitted biomarker response for hot and warm trials in the Open administration condition. Responses in the Hidden condition were not discernably (or statistically) different. Shaded areas show the standard error of the mean across participants. The solid lines show the fitted responses across trial amplitude estimates. The horizontal dashed line shows the threshold for Hot vs. Warm trials from Study 1.

Supplementary Table S1

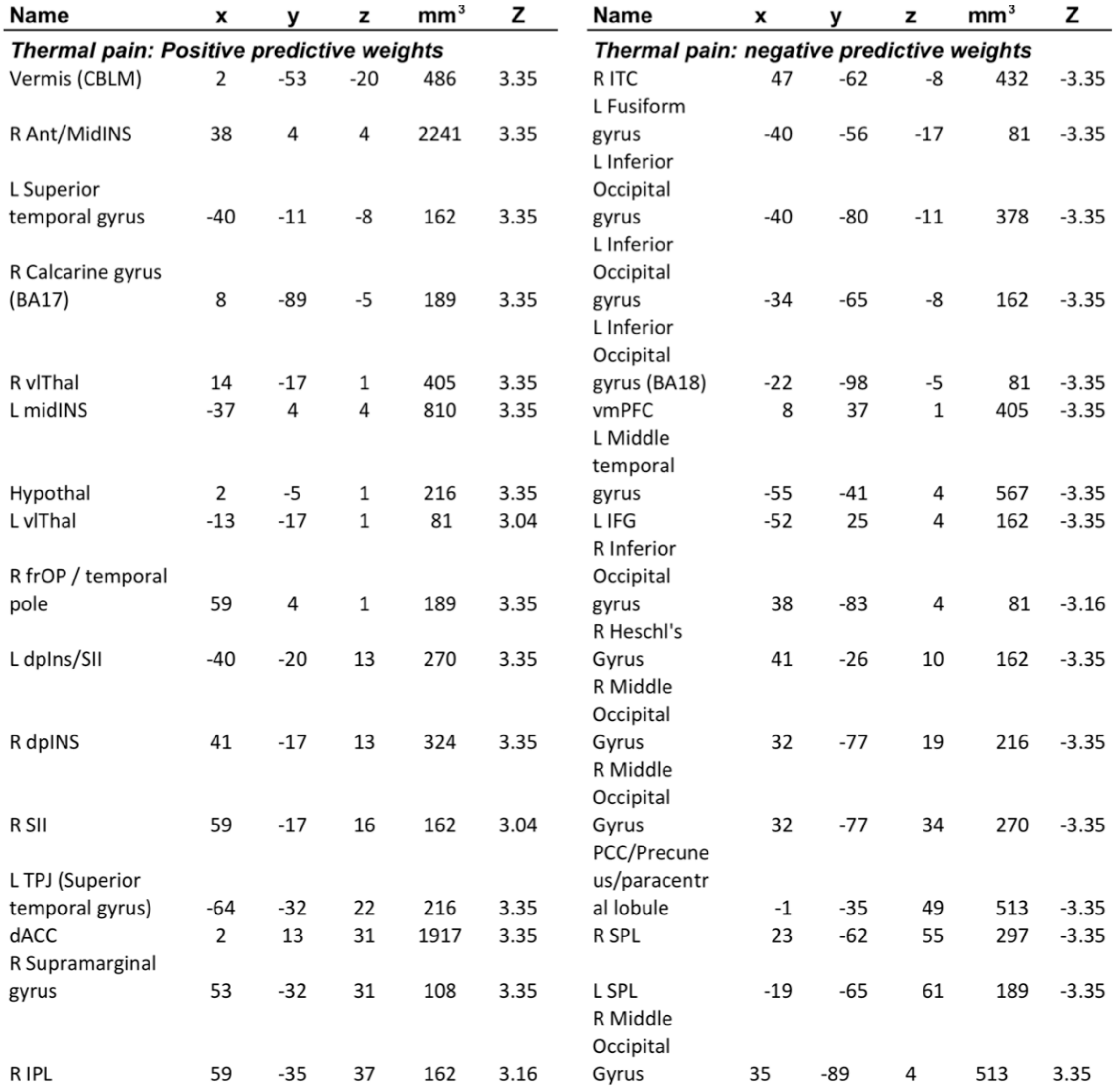

Name	x	y	z	mm³	Z	Name	x	y	z	mm³	Z
Thermal pain: Positive predictive weights						***Thermal pain: negative predictive weights***					
Vermis (CBLM)	2	-53	-20	486	3.35	R ITC	47	-62	-8	432	-3.35
R Ant/MidINS	38	4	4	2241	3.35	L Fusiform gyrus	-40	-56	-17	81	-3.35
L Superior temporal gyrus	-40	-11	-8	162	3.35	L Inferior Occipital gyrus	-40	-80	-11	378	-3.35
R Calcarine gyrus (BA17)	8	-89	-5	189	3.35	L Inferior Occipital gyrus	-34	-65	-8	162	-3.35
R vlThal	14	-17	1	405	3.35	L Inferior Occipital gyrus (BA18)	-22	-98	-5	81	-3.35
L midINS	-37	4	4	810	3.35	vmPFC	8	37	1	405	-3.35
Hypothal	2	-5	1	216	3.35	L Middle temporal gyrus	-55	-41	4	567	-3.35
L vlThal	-13	-17	1	81	3.04	L IFG	-52	25	4	162	-3.35
R frOP / temporal pole	59	4	1	189	3.35	R Inferior Occipital gyrus	38	-83	4	81	-3.16
L dpIns/SII	-40	-20	13	270	3.35	R Heschl's Gyrus	41	-26	10	162	-3.35
R dpINS	41	-17	13	324	3.35	R Middle Occipital Gyrus	32	-77	19	216	-3.35
R SII	59	-17	16	162	3.04	R Middle Occipital Gyrus	32	-77	34	270	-3.35
L TPJ (Superior temporal gyrus)	-64	-32	22	216	3.35	PCC/Precuneus/paracentral lobule	-1	-35	49	513	-3.35
dACC	2	13	31	1917	3.35	R SPL	23	-62	55	297	-3.35
R Supramarginal gyrus	53	-32	31	108	3.35	L SPL	-19	-65	61	189	-3.35
R IPL	59	-35	37	162	3.16	R Middle Occipital Gyrus	35	-89	4	513	3.35

Note. **Peak biomarker pattern weights from the machine learning analysis in Study 1.** The biomarker map was thresholded at $q < 0.05$ FDR for interpretation, based on a bootstrap test with 5000 bootstrap samples. Peak coordinates for positive and negative weights are listed in the left and right columns, respectively. Coordinates are reported in standard Montreal Neurologic Institute space. ACC, anterior cingulate cortex;CBLM: cerebellum; IFG, inferior frontal gyrus; INS, insula; IPL, inferior parietal lobule; ITC, inferior temporal cortex; OCC, occipital; frOP, frontal operculum; PCC, posterior cingulate cortex; PHCMP, parahippocampal cortex; PFC, prefrontal cortex; SMA, supplementary motor cortex; SPL, superior parietal lobule; STS, superior temporal sulcus; Thal, thalamus; TPJ, temporal-parietal junction; mvPFC, ventromedial prefrontal cortex. Prefixes: a, anterior; d, dorsal; l, lateral; m, medial; r, rostral; s, superior; v, ventral.

Supplementary Table S2.

Forced-choice discrimination test	**Discrimination**	**Effect size**		**Binomial test**
	Sens./Spec./PPV[h]	**AUC**	**d_a**	**P-value**
Study 1				
Painful vs. Warm[a]	100% (100-100%)	1.00	4.88	P < 0.001
Pain vs. Anticipation	100% (100-100%)	1.00	3.92	P < 0.001
Pain vs. Pain Recall	100% (100-100%)	1.00	2.29	P < 0.001
Conditions different by 3+ VAS units[f]	100% (100-100%)	1.00	3.91	P < 0.001
Conditions different by 2-3 VAS units	93% (84-100%)	0.97	2.17	P < 0.001
Conditions different by 1-2 VAS units	86% (76-95%)	0.86	1.15	P < 0.001
Conditions different by 0.5-1 VAS unit	69% (50-90%)	0.80	0.99	P = 0.26
Study 2				
Painful vs. Warm[c]	100% (100-100%)	1.00	3.12	P < 0.001
Painful (>125) vs. near-threshold (75-125)[e]	100% (100-100%)	1.00	2.77	P < 0.001
High (50-100) vs. low (0-50) warmth	100% (100-100%)	1.00	2.18	P < 0.001
49.3[g] vs. 48.3°C	90% (81%-97%)	0.93	1.71	P < 0.001
48.3 vs. 47.3°C	100% (100-100%)	1.00	2.00	P < 0.001
47.3 vs. 46.3°C	80% (67%-91%)	0.82	0.96	P = 0.001
46.3 vs. 45.3°C	67% (53%-81%)	0.77	0.77	P = 0.10
45.3 vs. 44.3°C	70% (56%-83%)	0.66	0.43	P = 0.04
Study 3				
Painful vs. Warm	93% (86-98%)	0.97	2.08	P < 0.001
Painful vs. Rejector Photo	95% (89-100%)	0.98	2.09	P < 0.001
Rejector Photo vs. Friend Photo	56% (43-69%)	0.66	0.49	P = 0.53
Study 4				
Hot vs. Warm, pre-drug	90% (79-100%)	0.97	1.76	P < 0.001
Hot vs. Warm, on-drug	76% (61-90%)	0.84	1.08	P < 0.05
Hot pre-drug vs. on-drug	76% (60-92%)	0.84	1.08	P < 0.05

Note. **Forced-choice classification performance across studies. *a*:** Painful conditions were defined as those > 44.5° C and >5.80 average VAS units, and Warm as < 44.5° C and <3.34 VAS units. ***b***: Study 2 was conducted on a scanner with a different field strength (3T), so a new threshold was estimated. ***c***: Participants made painful vs. non-painful judgments on each trial. ***d***: The threshold derived from Study 1 was applied. **e**: Continuous, 100-point VAS ratings for pain or warmth intensity (0-99 for warmth, 100-200 for pain). ***f***: Visual analogue scale (VAS) ratings on a continuous, 9-point scale. ***g***: Only 4 trials were included at 49.3° (cf. 11 trials for 44.3° and 15 trials for other conditions.) ***h***: For two-choice (forced-choice) discrimination, the decision threshold (for the difference between pairs) is 0, and the sensitivity, specificity, and positive predictive value (PPV) are the same, and are equal to the decision accuracy. AUC: Area under the Receiver Operating Characteristic curve, a threshold-independent measure of performance; chance is 0.5. PPV: Positive predictive value. d_a: Discriminability, a measure of effect size under a Gaussian model. Performance varies to some degree based on the number of trials per subject averaged to form condition maps in each study.

Supplementary Table S3

Pain/no pain test					Effect size		Binomial
	Thresh	**Sensitivity**	**Specificity**	**PPV**	**AUC**	d_a	**P-value**
Anterior insula							
Painful vs. Warm	0.44	83% (73-92%)	83% (73-92%)	83% (73-92%)	0.85	1.46	P < 0.001
Painful vs. Rejector Photo	0.48	80% (70-91%)	80% (69-90%)	80% (70-90%)	0.81	1.32	P < 0.001
Rejector Photo vs. Friend Photo	0.28	39% (26-50%)	78% (66-88%)	64% (47-79%)	0.53	0.15	P = 0.15
Anterior cingulate							
Painful vs. Warm	0.22	61% (49-74%)	85% (56-94%)	81% (69-92%)	0.75	1.02	P < 0.001
Painful vs. Rejector Photo	0.07	73% (62-84%)	76% (65-86%)	75% (64-86%)	0.78	1.15	P < 0.001
Rejector Photo vs. Friend Photo	0.12	22% (12-33%)	90% (82-98%)	69% (46-90%)	0.53	0.21	P = 0.32
S2/dorsal posterior insula							
Painful vs. Warm	0.19	73% (62-85%)	54% (40-67%)	61% (50-73%)	0.63	0.57	P = 0.02
Painful vs. Rejector Photo	0.12	73% (61-84%)	88% (78-96%)	86% (75-95%)	0.86	1.57	P < 0.001
Rejector Photo vs. Friend Photo	-0.58	59% (45-71%)	59% (46-71%)	59% (45-72%)	0.55	0.18	P = 0.15

Forced-choice test	**Discrimination**	**Effect size**		**Binomial**
	Sens./Spec./PPV[*a*]	**AUC**	d_a	**P-value**
Anterior insula				
Painful vs. Warm	88% (79-95%)	0.95	1.57	P < 0.001
Painful vs. Rejector Photo	83% (73-92%)	0.91	1.39	P < 0.001
Rejector Photo vs. Friend Photo	56% (44-68%)	0.59	0.25	P = 0.53
Anterior cingulate				
Painful vs. Warm	80% (70-91%)	0.86	1.12	P < 0.001
Painful vs. Rejector Photo	80% (70-90%)	0.89	1.20	P < 0.001
Rejector Photo vs. Friend Photo	61% (48-73%)	0.62	0.34	P = 0.21
S2/dorsal posterior insula				
Painful vs. Warm	73% (61-84%)	0.73	0.69	P < 0.01
Painful vs. Rejector Photo	90% (82-98%)	0.97	1.71	P < 0.001
Rejector Photo vs. Friend Photo	59% (46-71%)	0.61	0.31	P = 0.35

Note. **Pain/no-pain classification performance for single, selected regions in Study 3.** The biomarker response estimated from weights only with each single, a priori region of interest were used to evaluate performance. ***a***: For two-choice (forced-choice) discrimination, the decision threshold (for the difference between pairs) is 0, and the sensitivity, specificity, and positive predictive value (PPV) are the same, and are equal to the decision accuracy. AUC: Area under the Receiver Operating Characteristic curve, a threshold-independent measure of performance. PPV: Positive predictive value. d_a: Discriminability, a measure of effect size under a Gaussian model. 95% confidence intervals are shown in parentheses, and were estimated using bootstrap resampling with 1000 samples per test.

References

1. Atlas LY, Bolger N, Lindquist MA, Wager TD. Brain Mediators of Predictive Cue Effects on Perceived Pain. J Neurosci 2010;30:12964 –77.

2. Buhle J, Wager TD. Performance-dependent inhibition of pain by an executive working memory task. Pain 2010.

3. Ashburner J, Friston KJ. Unified segmentation. NeuroImage 2005;26:839-51.

4. Lund TE, Madsen KH, Sidaros K, Luo WL, Nichols TE. Non-white noise in fMRI: does modelling have an impact? NeuroImage 2006;29:54-66.

5. Handwerker DA, Gonzalez-Castillo J, D'Esposito M, Bandettini PA. The continuing challenge of understanding and modeling hemodynamic variation in fMRI. NeuroImage 2012.

6. Aguirre G, Zarahn E, D'Esposito M. The variability of human, BOLD hemodynamic responses. NeuroImage 1998;8:360-9.

7. Thomas CG, Harshman RA, Menon RS. Noise reduction in BOLD-based fMRI using component analysis. NeuroImage 2002;17:1521-37.

8. Tohka J, Foerde K, Aron AR, Tom SM, Toga AW, Poldrack RA. Automatic independent component labeling for artifact removal in fMRI. NeuroImage 2008;39:1227-45.

9. Tibshirani R. Regression shrinkage and selection via the Lasso. Journal of the Royal Statistical Society, Series B 1996;58:267-88.

10. Wager TD, Atlas LY, Leotti LA, Rilling JK. Predicting Individual Differences in Placebo Analgesia: Contributions of Brain Activity during Anticipation and Pain Experience. J Neurosci 2011;31:439-52.

11. Yarkoni T, Poldrack RA, Nichols TE, Van Essen DC, Wager TD. Large-scale automated synthesis of human functional neuroimaging data. Nature Methods 2011.

12. Baliki MN, Geha PY, Apkarian AV. Parsing pain perception between nociceptive representation and magnitude estimation. J Neurophysiol 2009;101:875-87.

13. Lindquist MA, Loh JM, Atlas L, Wager TD. Modeling the hemodynamic response function in fMRI: Efficiency, bias and mis-modeling. NeuroImage 2009;45:S187-S98.

14. Wager TD, Rilling JK, Smith EE, et al. Placebo-induced changes in FMRI in the anticipation and experience of pain. Science 2004;303:1162-7.

15. Bornhovd K, Quante M, Glauche V, Bromm B, Weiller C, Buchel C. Painful stimuli evoke different stimulus-response functions in the amygdala, prefrontal, insula and somatosensory cortex: a single-trial fMRI study. Brain 2002;125:1326-36.

16. Koyama Y, Koyama T, Kroncke AP, Coghill RC. Effects of stimulus duration on heat induced pain: the relationship between real-time and post-stimulus pain ratings. Pain 2004;107:256-66.

17. Rish I, Cecchi G, Baliki M. Sparse regression models of pain perception. Brain Informatics 2010.

18. Grosenick L, Greer S, Knutson B. Interpretable classifiers for FMRI improve prediction of purchases. IEEE Trans Neural Syst Rehabil Eng 2008;16:539-48.

19. Smola AJ, Schölkopf B. A tutorial on support vector regression. Statistics and computing 2004;14:199-222.

20. Kross E, Berman MG, Mischel W, Smith EE, Wager TD. Social rejection shares somatosensory representations with physical pain. Proceedings of the National Academy of Sciences 2011;108:6270-5.

21. Kross E, Davidson M, Weber J, Ochsner K. Coping with emotions past: the neural bases of regulating affect associated with negative autobiographical memories. Biol Psychiatry 2009;65:361-6.

22. Wager TD, Scott DJ, Zubieta JK. Placebo effects on human mu-opioid activity during pain. Proceedings of the National Academy of Sciences 2007;104:11056-61.

23. Atlas LY, Whittington RA, Lindquist MA, Wielgosz J, Sonty N, Wager TD. Dissociable influences of opiates and expectations on pain. J Neurosci 2012;32:8053-64.

24. Minto CF, Schnider TW, Egan TD, et al. Influence of age and gender on the pharmacokinetics and pharmacodynamics of remifentanil. I. Model development. Anesthesiology 1997;86:10-23.

25. Minto CF, Schnider TW, Shafer S. Pharmacokinetics and pharmacodynamics of remifentanil. II. Model application. Anesthesiology 1997;86:24-33.

26. Apkarian AV, Darbar A, Krauss BR, Gelnar PA, Szeverenyi NM. Differentiating cortical areas related to pain perception from stimulus identification: temporal analysis of fMRI activity. J Neurophysiol 1999;81:2956.

27. Wanigasekera V, Lee MC, Rogers R, Hu P, Tracey I. Neural correlates of an injury-free model of central sensitization induced by opioid withdrawal in humans. J Neurosci 2011;31:2835-42.

28. Wise RG, Williams P, Tracey I. Using fMRI to quantify the time dependence of remifentanil analgesia in the human brain. Neuropsychopharmacology 2004;29:626-35.
29. Buhle JT, Stevens BL, Friedman JJ, Wager TD. Distraction and Placebo: Two Separate Routes to Pain Control. Psychol Sci 2012.
30. Bantick SJ, Wise RG, Ploghaus A, Clare S, Smith SM, Tracey I. Imaging how attention modulates pain in humans using functional MRI. Brain 2002;125:310-9.
31. Apkarian AV, Hashmi JA, Baliki MN. Pain and the brain: Specificity and plasticity of the brain in clinical chronic pain. Pain 2011;152:S49-S64.
32. Borsook D, Becerra L, Hargreaves R. Biomarkers for chronic pain and analgesia. Part 1: the need, reality, challenges, and solutions. Discovery medicine 2011;11:197-207.
33. Borsook D, Becerra L, Hargreaves R. Biomarkers for chronic pain and analgesia. Part 2: how, where, and what to look for using functional imaging. Discovery medicine 2011;11:209-19.
34. McGonigle DJ, Howseman AM, Athwal BS, Friston KJ, Frackowiak RS, Holmes AP. Variability in fMRI: an examination of intersession differences. NeuroImage 2000;11:708-34.
35. Glover GH, Mueller BA, Turner JA, et al. Function biomedical informatics research network recommendations for prospective multicenter functional MRI studies. J Magn Reson Imaging 2012.
36. Hoge RD. Calibrated fMRI. NeuroImage 2012.
37. Bjornsdotter M, Loken L, Olausson H, Vallbo A, Wessberg J. Somatotopic organization of gentle touch processing in the posterior insular cortex. J Neurosci 2009;29:9314-20.
38. Haynes JD, Rees G. Predicting the orientation of invisible stimuli from activity in human primary visual cortex. Nat Neurosci 2005;8:686-91.
39. Kamitani Y, Tong F. Decoding the visual and subjective contents of the human brain. Nat Neurosci 2005;8:679-85.
40. Sabuncu MR, Singer BD, Conroy B, Bryan RE, Ramadge PJ, Haxby JV. Function-based intersubject alignment of human cortical anatomy. Cereb Cortex 2010;20:130-40.
41. Flor H, Elbert T, Knecht S, et al. Phantom-limb pain as a perceptual correlate of cortical reorganization following arm amputation. Nature 1995;375:482-4.
42. Donahue MJ, Hoogduin H, van Zijl PC, Jezzard P, Luijten PR, Hendrikse J. Blood oxygenation level-dependent (BOLD) total and extravascular signal changes and DeltaR2* in human visual cortex at 1.5, 3.0 and 7.0 T. NMR Biomed 2011;24:25-34.
43. Davis TL, Kwong KK, Weisskoff RM, Rosen BR. Calibrated functional MRI: mapping the dynamics of oxidative metabolism. Proc Natl Acad Sci U S A 1998;95:1834-9.